Check for updates

Nano-liposome encapsulation of adenosine and cordycepin from *Cordyceps militaris*: preparation, characterization, stability, and *in vitro* digestion evaluation†

Nguyen Quynh Dao, [ID] [ab] Nguyen Thanh Tan, [ID] [a] Nguyen Ba Thanh, [ID] [a]
Le Minh Hung,[c] Nguyen Van My, [ID] [d] Nguyen Minh Hai, [ID] [e] Nguyen Phuong Tuyen,[b]
Nguyen Quoc Thang, [ID] [f] Tran Chi Dung [ID] [f] and Tran Quang Hieu [ID] *[bg]

This study aimed to develop and characterize a nano-liposome system encapsulating adenosine (ADE) and cordycepin (COR) from the aqueous extract of *Cordyceps militaris* to enhance their bioavailability and stability. The liposomes were prepared using the solvent injection method, yielding an average particle size of 100.3 nm and encapsulation efficiencies of $72.7 \pm 3.2\%$ for ADE and $75.7 \pm 3.8\%$ for COR. The system demonstrated excellent stability over 28 days under refrigerated conditions, with minimal changes in particle size and zeta potential. Additionally, the nano-liposomes exhibited superior antioxidant activity compared to the raw extract, neutralizing 84% of DPPH free radicals at a concentration of 6.25 mg mL^{-1}. The liposome LCMs shell effectively protected ADE and COR in the simulated gastric environment, with cumulative release of less than 20%, while precisely controlling their release in the intestinal environment, achieving over 85%. These findings underscore the potential of this nano-liposome system for applications in functional foods and pharmaceuticals, offering a promising approach to maximize the health benefits of *Cordyceps militaris*.

Sustainability spotlight

This study highlights the development of a nano-liposome delivery system for adenosine and cordycepin from *Cordyceps militaris*, emphasizing its potential to enhance the bioavailability and stability of bioactive compounds while minimizing environmental impact. The optimized solvent injection method used in this research reduces the need for harsh chemicals and energy-intensive processes, aligning with green chemistry principles. Additionally, the use of natural extracts and biodegradable liposome materials supports sustainable and eco-friendly approaches in pharmaceutical and functional food applications. This work contributes to the advancement of sustainable technologies by offering a scalable and environmentally responsible platform for the delivery of bioactive compounds, ultimately promoting health and well-being without compromising planetary health.

[a]Institute of Biotechnology and Food Technology, Industrial University of Ho Chi Minh City, 12 Nguyen Van Bao Street, Ward 1, Go Vap District, Ho Chi Minh City 700000, Vietnam

[b]Faculty of Food Technology – Saigon Technology University, 180 Cao Lo Street, Ward 4, District 8, Ho Chi Minh City 700000, Vietnam. E-mail: hieu.tranquang@stu.edu.vn

[c]Sub-Institute of Agricultural Engineering and Post-Harvest Technology, 54 Tran Khanh Du, Ho Chi Minh City 700000, Vietnam

[d]Chemistry Faculty, Ho Chi Minh University of Education, 280 An Duong Vuong, District 5, Ho Chi Minh City, 700000, Vietnam

[e]Faculty of Chemical and Food Technology, HCMC University of Technology and Education, Vo Van Ngan Street, Thu Duc City, Ho Chi Minh City 700000, Vietnam

[f]Faculty of Chemical Engineering, Industrial University of Ho Chi Minh City, 12 Nguyen Van Bao, Go Vap, Ho Chi Minh City 700000, Vietnam

[g]Basic Sciences Department, Saigon Technology University, 180 Cao Lo Street, Ward 4, District 8, Ho Chi Minh City 700000, Vietnam

† Electronic supplementary information (ESI) available. See DOI: https://doi.org/10.1039/d5fb00146c

1. Introduction

Cordyceps militaris, commonly known as cultivated *Cordyceps*, has a long history in traditional medicine for enhancing health and supporting the treatment of various diseases.[1] Among its bioactive components, adenosine (ADE) and cordycepin (COR) stand out due to their significant health benefits, including anti-inflammatory, antioxidant, and immune-boosting properties.[2,3] ADE, a naturally occurring nucleoside, plays a crucial role in physiological processes like energy metabolism and blood circulation. It's effective in reducing inflammation, alleviating pain, protecting cells from damage, and treating arrhythmias and ischemic disorders.[4] COR, or 3′-deoxyadenosine, has garnered attention for its antimicrobial, antiviral, and anti-cancer properties, inhibiting the growth of cancer cells and bacteria while enhancing the immune response.[5] Deng *et al.* demonstrated that COR directly inhibits the growth and

proliferation of CT26 colon cancer cells, inducing apoptosis, and *in vivo* studies have shown that cordycepin administration can significantly suppress tumor growth and reduce colon cancer spread.[6] Zhang *et al.* reported that COR can suppress colon cancer cell proliferation, likely *via* the MYC/miR-26a pathway, supporting its potential for colon cancer treatment.[7] These findings suggest that targeted delivery of functional foods containing ADE and COR from *Cordyceps militaris* extract to the intestine may offer therapeutic support in colon cancer treatment. The potential of *Cordyceps* extracts extends beyond colon cancer; for example, Cai *et al.* demonstrated that *Cordyceps* extracts inhibit breast cancer cell metastasis by down-regulating metastasis-related cytokines.[8] However, COR can degrade due to temperature, light, and especially H^+ ions. Tang reported that at pH 1 and 3, COR retention decreased rapidly during 36 hours of storage, dropping to 79.83% at pH 1, while remaining above 90% at higher pH values.[9] ADE and COR are also susceptible to degradation by adenosine deaminase (ADA), an enzyme also known as adenosine aminohydrolase, found in plants, bacteria, and humans.[10] ADA is a zinc-containing metalloenzyme (41 kDa) that deaminates ADE and 2′-deoxyadenosine into inosine and 2′-deoxyinosine during purine metabolism.[11] Similarly, COR is deaminated by ADA into cordycepin 3′-deoxyinosine, reducing its concentration. Oxidative stress can also accelerate COR degradation,[12] and Lee *et al.* showed that in mice, COR is rapidly converted into 3′-deoxyinosine and ultimately into cordycepin 5′-triphosphate in the circulatory system.[13] Furthermore, the relatively small size of ADE and COR leads to rapid clearance and suboptimal distribution, limiting their therapeutic effects. To address these challenges, researchers are actively developing nano-carriers that offer a promising approach to encapsulate and protect these active ingredients from degradation, while enabling targeted delivery. Among the available nano-carriers, nano-liposomes have attracted significant attention as potential drug carriers. Nano-liposomes are nanoscale delivery systems composed of lipids that can encapsulate and protect bioactive compounds, maintaining their activity during transport.[14,15] Their small size (20–200 nm) enhances cellular membrane permeability, improving compound absorption. Liposomes increase the solubility of poorly soluble compounds, allow for controlled release, reduce toxicity, and enable targeted delivery while protecting active compounds from degradation in the digestive system.[16]

To date, limited studies have explored the encapsulation of *Cordyceps militaris* extract, with examples including nanoemulsions,[17] and liposomes.[18,19] To our knowledge, this study is the first to report the co-encapsulation of both an ADE and COR-rich extract from *Cordyceps militaris* aqueous extract into liposomes *via* the solvent injection method. We provide a comprehensive investigation of factors influencing liposome formation, a thorough characterization of the resulting nanosuspension using techniques such as DLS, TEM, zeta potential, and IR spectroscopy, and an examination of factors affecting its stability. Furthermore, this is the first evaluation in a simulated digestive system demonstrating that the nanosystem protects ADE and COR under simulated gastric conditions and facilitates their controlled release in the intestinal environment.

These findings offer a novel strategy for developing *Cordyceps militaris*-derived functional food ingredients, enabling the targeted delivery of the valuable active ingredients ADE and COR to the intestinal tract to maximize their biological activity.

2. Materials and methods

2.1. Materials and chemicals

Cordyceps militaris was sourced from Thien An Cordyceps Co., Ltd (Go Cong Tay, Tien Giang, Vietnam). The fruiting bodies were collected after a 4-month cultivation period, freeze-dried, ground into powder, packaged, and transported to the laboratory for further analysis. ADE (lot: 4-SCC-138-1, 98%) and COR (lot: 11-XJZ-169-1, 98%) were purchased from TRC (Toronto, Canada). Soybean lecithin (LC) and Tween 80 were supplied by Macklin (China). Dichloromethane, ethanol, diethyl ether, trolox, and 2,2-diphenyl-1-picrylhydrazyl (DPPH) were obtained from Sigma-Aldrich (Merck, Germany). All other chemicals used were of analytical grade.

2.2. Equipment

The study utilized a range of advanced equipment to ensure precise and reproducible results. An ultrasonic bath (Ultrasound CB S-100H, Germany) was employed for sample preparation, while a probe sonicator (VCX-750, Sonic, USA) was used for the homogenization of lipid suspensions. The surface charge and stability of the nano-liposomes were characterized using a zeta potential analyzer (Zetasizer ZS90, Malvern, UK), and their particle size distribution was determined with a particle size analyzer (Horiba SZ-100, Japan). Structural analysis of the liposomes was performed using a Fourier-transform infrared (FTIR) spectrometer (FT/IR-6600, Jasco, USA), and the antioxidant activity of the extracts was evaluated with a UV-vis spectrophotometer (Genesis 10, Thermo, USA). All equipment met standard laboratory requirements and ensured the reliability of the experimental data.

2.3. UHPLC-MS/MS analysis for quantitation of ADE, COR

2.3.1. Mobile phase and mass spectrometry conditions. The quantification of ADE and COR was carried out using UHPLC-MS/MS (Ultimate 3000, Thermo Fisher Scientific, Germany) equipped with a HILIC Silica 3 μm, 2.1 × 50 mm column (Atlantis). The mobile phase consisted of Phase A (ACN + 100 mM HCOOH) and Phase B (deionized water + 0.5% HCOOH). A linear gradient was established as follows: 0 min (10% B) → 3 min (40% B) → 6.0 min (40% B) → 6.1 min (10% B) → 12 min (10% B), with a constant flow rate of 0.3 mL min^{-1} throughout the chromatographic analysis. This method ensured efficient separation and accurate quantification of the target analytes.

The Selected Reaction Monitoring (SRM) program of TraceFinder 3.3 software was employed to identify and quantify the analytes with high specificity and sensitivity. The Heated Electrospray Ionization (H-ESI) source was operated in positive ion mode (H-ESI (+)) with a spray voltage of 3500 V. To ensure efficient ionization, desolvation, and ion transfer, the vaporizer

temperature and ion transfer tube temperature were maintained at 300 °C. The sheath gas flow rate was optimized to 40 arbitrary units (arb), while the auxiliary gas flow rate was set to 5 arbs to enhance ion stability and signal intensity. A collision-induced dissociation (CID) gas pressure of 2 mTorr was maintained to ensure optimal fragmentation of the analytes for accurate identification and quantification. The SRM parameters were as follows: for ADE, the precursor ion (m/z) was 268.122, and product ions of 94.097, 119.058, and 136.058 were monitored with collision energies of 42.107 V, 43.674 V, and 17.837 V, respectively, with the product ion at m/z 136.058 designated as the quantitation ion. For COR, the precursor ion (m/z) was 252.152, and product ions of 94.111, 119.04, and 136.04 were monitored with collision energies of 39.275 V, 42.511 V, and 16.118 V, respectively, with the product ion at m/z 136.04 designated as the quantitation ion.

2.3.2. Calibration curves. The concentrations of ADE and COR were quantified using calibration curves generated from peak area *versus* analyte concentration, as detailed in our previous work.[20] Working standards, with concentrations ranging from 10 to 1000 μg L^{-1} (10, 20, 50, 100, 200, 500, and 1000 μg L^{-1}), were prepared *via* serial dilution of a 1.0 mg mL^{-1} primary stock solution containing both analytes in ACN. The resulting linear regression equations were: $y = 1.993 \times 10^3 x - 9.638 \times 10^4$ ($R^2 = 0.9991$) for ADE, and $y = 2.297 \times 10^3 x + 1.756 \times 10^4$ ($R^2 = 0.9992$) for COR. The limit of quantification (LOQ) for both ADE and COR was determined to be 10.0 μg L^{-1}.

Samples were diluted with acetonitrile (dilution factor adjusted based on ADE and COR content), filtered through a 0.22 μm filter, transferred to 1.5 mL amber LC vials, and analyzed by UPLC-MS/MS. The injection volume was 2.0 μL, and samples were introduced *via* the autosampler under optimized conditions.

2.4. Preparation of LCMs

2.4.1. Extraction of *Cordyceps militaris*. In this study, *Cordyceps militaris* was extracted using an ultrasonic bath-assisted extraction method (Ultrasound CB S-100H, Germany) with water as the solvent. The extraction parameters were optimized as follows: a solvent-to-material ratio of 1 : 20, a temperature of 45 °C, and an ultrasonic power of 300 W for 30 min. After extraction, the solution was filtered through a 0.45 μm membrane to obtain a clear extract with a Brix level of 3.5. The concentrations of ADE and COR in the extract were quantified using UHPLC-MS/MS. The determined concentrations of ADE and COR were 77.71 ± 2.83 mg L^{-1} and 120.81 ± 3.44 mg L^{-1}, respectively.

2.4.2. Preparation of nano-liposome system (LCMs). The preparation of the nano-liposome system (LCMs) was adapted from previous work with some modifications to suit the experimental conditions.[21] Briefly, 0.4 g of soybean lecithin (LC) was weighed and dissolved in 25 mL of a mixture of ethanol and dichloromethane (4 : 1 v/v) under magnetic stirring at 300 rpm. This lipid solution was then injected into 100 mL of *Cordyceps militaris* extract containing ADE, COR, and 1.5% Tween 80 in phosphate buffer (pH 7.4). The mixture was stirred at 800 rpm

and heated to 80 °C for 30 min to evaporate the organic solvents. Subsequently, the system was sonicated at 60% power for 1.0 min using a probe sonicator (VCX-750, Sonic, USA) to form the LCMs. Finally, the suspension was filtered through filter paper to obtain the nano-LCMs dispersion.

Several factors influencing the encapsulation efficiency (EE%) and average particle size (D, nm) were investigated, including the dropping rate, ultrasonic power, and sonication time.

2.5. Encapsulation efficiency evaluation

The encapsulation efficiency of ADE and COR into liposomes was determined using an ultrafiltration method adapted from previously described procedures.[18,19,22] Briefly, 2.0 mL of the LMCs suspension was loaded into Amicon® Ultra-15, 10 kDa centrifugal filter tubes (Merck Millipore Ltd, Darmstadt, Germany) equipped with Ultracel® regenerated cellulose membranes. These tubes were then centrifuged at 10 000×g for 1.0 h to separate unencapsulated ADE and COR from the LMCs. The filtrate, containing the free ADE and COR, was collected. This sample solution was then diluted with acetonitrile (with the dilution factor adjusted depending on the initial concentration of ADE and COR) and filtered through a 0.22 μm membrane into a 1.5 mL amber LC vial. Finally, a 2.0 μL aliquot of this processed sample was injected into the UHPLC-MS/MS for quantitation of ADE and COR content.

The encapsulation efficiency (EE%) was calculated using the eqn (1):

$$EE(\%) = \frac{C_o - C_f}{C_o} \times 100 \tag{1}$$

where, C_o represents the initial concentration of ADE/COR used for liposome preparation and C_f denotes the amount of ADE/COR measured in the filtrate after the centrifugation.

2.6. LCMs physicochemical characterization

The characteristics of the nano-LCMs system were determined by evaluating the average particle size (Z-average, nm), polydispersity index (PDI, a.u.), zeta potential (ZP, mV), and particle morphology. The particle size and PDI were measured using Dynamic Light Scattering (DLS) on a Horiba SZ-100 instrument (Japan). The surface charge of the nanoparticles (zeta potential) was determined using a Zetasizer ZS90 (Malvern, UK). The morphology of the nano-liposomes was observed using Transmission Electron Microscopy (TEM) (HT 7700, Hitachi, Ltd, Japan). Additionally, FT-IR spectroscopy was employed to identify the characteristic functional group vibrations of the extract and the nano-system, performed on an FT/IR-6600 spectrometer (Jasco, USA). All measurements were conducted at the Institute of Materials Science and Applications, District 12, Ho Chi Minh City.

2.7. Stability evaluation

The stability of the nano-LCMs system is a critical factor for its practical application. To evaluate this, the effects of temperature, NaCl concentration, and storage time were systematically

investigated. Key parameters, including particle size, PDI, and EE%, were monitored to assess the system's stability under various conditions. These analyses provided valuable insights into the robustness of the nano-system, which is essential for its potential use in pharmaceutical and nutraceutical applications.

2.7.1. Effect of temperature. To evaluate the thermal stability of the nano-LCMs system, 5.0 mL of the nano-LCMs dispersion was placed into a heat-resistant glass beaker and heated at different temperatures: room temperature (control, 25 °C), 50 °C, and 90 °C for 10 min. After cooling, the particle size was measured using Dynamic Light Scattering (DLS).

2.7.2. Effect of NaCl concentration. The effect of ionic strength on the stability of the nano-LCMs system was investigated by mixing 5.0 mL of the nano-LCMs dispersion with 0.1 mL, 0.5 mL, and 1.0 mL of 1.0 M NaCl solution. After 30 min, the particle size was measured using DLS.

2.7.3. Effect of storage time. To assess the long-term stability of the nano-LCMs system, 5.0 mL of the LCMs dispersion was transferred into capped test tubes and stored at room temperature (25 °C) and cold temperature (4 °C). The particle size and EE% were measured at intervals of 7, 14, 21, and 28 days. Each experiment was repeated three times for each condition to obtain the mean value and standard deviation. The retention rate of ADE and COR was calculated using the eqn (2):

$$RR(\%) = \frac{EE_i}{EE_o} \times 100 \qquad (2)$$

In the formula, EE_o and EE_i represent the encapsulation efficiency at the initial time and time of investigation, respectively.

2.8. In vitro simulated digestion study

In order to evaluate the ability of the LCMs nano-system to protect the active compounds ADE and COR from digestive factors present in the gastric system, such as enzymes and acidic media, as well as their release in the intestinal environment, the in vitro release of ADE and COR from LMCs was investigated using a simulated digestion model. This model consisted of two phases: a simulated gastric fluid (SGF) phase and a small intestinal fluid (SIF) phase.[23,24]

Digestive fluid components were prepared following the procedures described in the previous publications of Liu et al.[25] and Ji et al.[26] with slight adjustments. Specifically, SGF was composed of sodium chloride (2.0 g L^{-1}) and pepsin (3.2 g L^{-1}), and the pH was adjusted to 1.2 using hydrochloric acid and sodium hydroxide. SIF contained calcium chloride (1.2 mM), sodium chloride (15 mM), pancreatin (4.76 g L^{-1}), and bile salts (5.16 g L^{-1}); the pH was adjusted to 7.0 using hydrochloric acid and sodium hydroxide. All simulated digestive fluids and liposomes were preheated to 37 °C prior to use.

The in vitro simulated digestion process was conducted in two stages to mimic gastrointestinal conditions. First, 10 mL of LCMs were mixed with 10 mL of SGF to simulate gastric digestion for 2 hours. Following this, 5 mL of the gastric fluid mixture was taken, and the pH adjusted to 7.0 before adding 5 mL of SIF to simulate small intestinal digestion. The entire

simulated digestion process was performed in a shaking water bath at 37 °C to mimic gastrointestinal peristalsis.

To assess the release of ADE and COR from LMCs, 1.0 mL of the digestive mixture was collected at specific time intervals (15, 30, 60, 90, and 120 min for the SGF model and 135, 150, 180, 210, and 240 min for the SIF model) and immediately cooled in an ice bath to inhibit enzyme activity. Each sample was then centrifuged using Amicon® Ultra-15, 10 kDa centrifugal filter tubes at 4 °C for 1.0 hour (10 000×g). The filtrate was collected and diluted in acetonitrile, and the concentrations of ADE and COR were then determined using UHPLC-MS/MS, as described in Section 2.4. The cumulative release rate (%) of ADE and COR was calculated and plotted as a function of time using eqn (3)

$$\text{Culmulative release rate}(\%) = \sum_0^t \frac{m_t}{m_o} \times 100 \qquad (3)$$

where m_o is the initial amount of ADE and COR encapsulated in LCMs and m_t denotes the cumulative amount of released ADE, COR in digestive medium at various sampling time points.

2.9. Evaluation of antioxidant activity

The antioxidant activity of the samples was assessed using the DPPH (2,2-diphenyl-1-picrylhydrazyl) free radical scavenging assay, adapted from previously published methods with modifications to suit the experimental conditions.[22,27,28]

2.9.1. Preparation of trolox standard curve. A Trolox standard curve was constructed by adding 0.1 mL of Trolox solution at concentrations of 200, 400, 600, 800, and 1000 μM into separate test tubes. Then, 3.9 mL of DPPH solution (6×10^{-5} M) was added to each tube, resulting in final Trolox concentrations of 5.0, 10.0, 15.0, 20.0, and 25.0 μg mL^{-1}. The mixtures were vortexed for 20 seconds and incubated in the dark at room temperature for 60 min. The absorbance was measured at a wavelength of 517 nm using a UV-vis spectrophotometer (Genesys 10s, Thermo, USA).

2.9.2. Sample analysis. A volume of 0.1 mL of the sample solution at concentrations of 25, 50, 125, 250, and 500 mg mL^{-1} was mixed with 3.9 mL of DPPH solution, following the same procedure as for the Trolox standard. This resulted in final sample concentrations of 0.625, 1.25, 3.125, 6.25, and 12.5 mg mL^{-1} in the test solutions. The antioxidant activity was evaluated based on the percentage of radical scavenging activity (RSA, %) and the IC50 value, which represents the concentration required to scavenge 50% of the DPPH radicals. The antioxidant activity was calculated using the eqn (4):

$$RSA(\%) = \left(1 - \frac{A_{blank}}{A_{sample}}\right) \times 100 \qquad (4)$$

where: RSA (%) represents the radical scavenging activity. A_{blank} is the absorbance of the blank sample (DPPH solution without the test sample). A_{sample} is the absorbance of the test sample (DPPH solution with the test sample).

2.10. Data analysis

The results are expressed as mean ± standard deviation (SD). All experiments were repeated at least three times to calculate the

mean and standard deviation using Microsoft Excel. Statistical analysis was performed using one-way ANOVA followed by Tukey's multiple comparisons test at a significance level of 5.0% ($p < 0.05$). Graphs and figures were processed and plotted using Origin 2025 (Education version).

3. Result and discussion

3.1. Factor effect on liposome formulation

3.1.1. Effect of lecithin concentration. The concentration of lecithin is a critical factor influencing the stability and encapsulation efficiency of the liposome system.[29] In this study, the concentration of LC relative to the aqueous phase was systematically investigated at 0.1%, 0.2%, 0.4%, 0.6%, 0.8%, and 1.0% (w/v). The results demonstrated that at a LC concentration of 0.4% (w/v), the system exhibited high stability over a 7-day storage period under ambient conditions. This stability can be attributed to the optimal lipid-to-water ratio, which ensures the formation of well-structured liposomes without excessive aggregation. Conversely, at higher LC concentrations (>0.4%), the system experienced phase separation, likely due to excessive lipid aggregation, which disrupted the uniformity of the liposome structure. On the other hand, at lower LC concentrations (<0.4%), the EE% dropped below 60%, indicating insufficient lipid content to effectively encapsulate the

bioactive compounds. This reduction in EE% at lower concentrations underscores the importance of adequate lipid levels for successful encapsulation. Based on these results, a LC concentration of 0.4% (w/v) was selected for subsequent experiments.

3.1.2. Injection rate. In the preparation of liposomes using the solvent injection method, the dropping rate of the solvent into the aqueous phase plays a crucial role in controlling the particle size and uniformity of the system.[30] Fig. 1A and Table S1† demonstrate that different dropping rates (0.4, 0.6, 0.8, and 1.0 mL min^{-1}) significantly influence the particle size and uniformity of the liposomes. Specifically, a dropping rate of 0.6 mL min^{-1} was identified as optimal, producing liposomes with an average size of 122.3 nm and a low standard deviation (4.2 nm), indicative of a uniform and stable size distribution. In contrast, a dropping rate of 0.4 mL min^{-1} yielded a liposome size of 124.3 nm, which was not statistically different from that obtained at 0.6 mL min^{-1}. However, increasing the dropping rate to 0.8 and 1.0 mL min^{-1} resulted in a significant increase in particle size to 146.0 nm and 180.7 nm, respectively. These differences were analyzed using one-way ANOVA followed by Tukey's test, confirming statistical significance at $p < 0.05$. These findings underscore the strong influence of the injection rate on liposome formation and size. Additionally, it has been reported that a low injection rate may accelerate lipid oxidation,
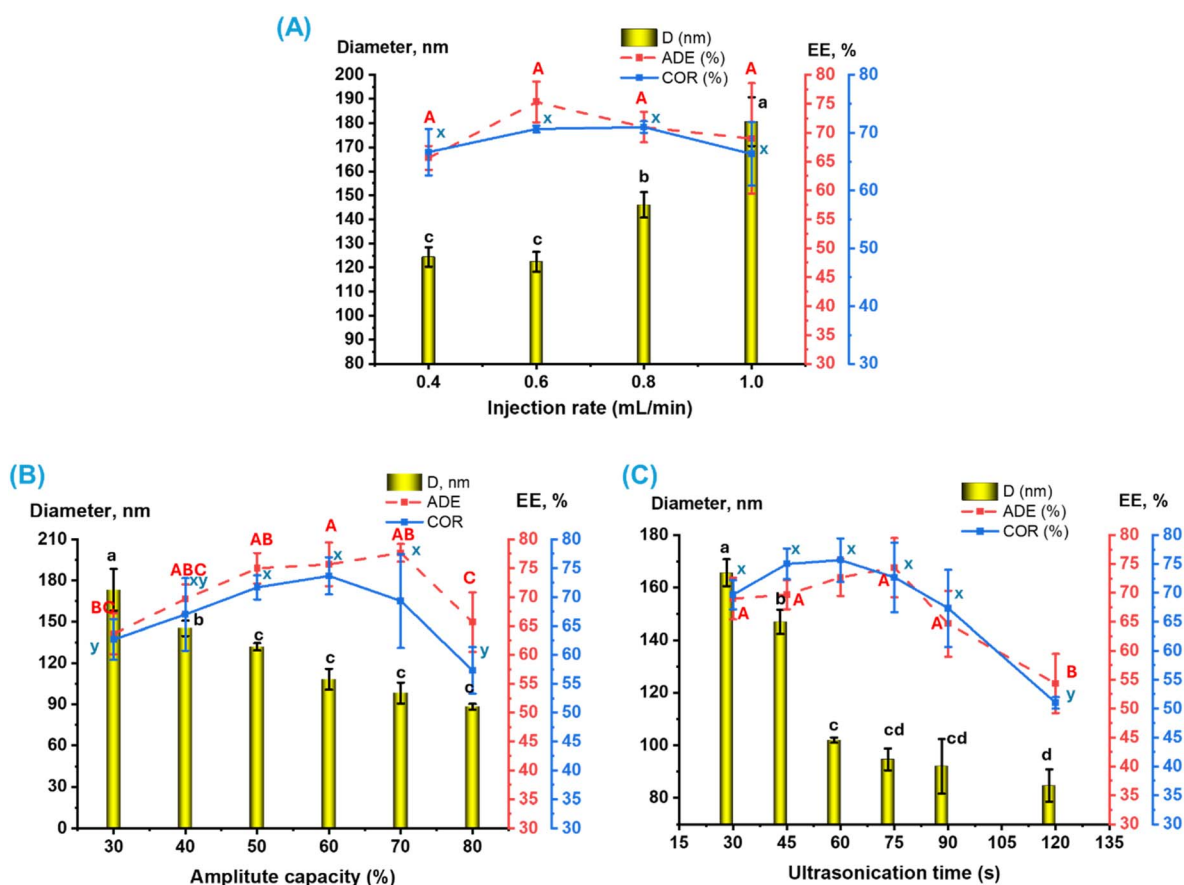

Fig. 1 Factors influencing the properties of the LCMs system: (A) injection rate, (B) ultrasonic power, and (C) sonication time. Different letters indicate statistically significant differences at a confidence level of $p < 0.05$.

Sustainable Food Technology

while a high injection rate can lead to a polydisperse distribution of liposomes, potentially due to secondary nucleation, which contributes to increased droplet size.[31,32]

Furthermore, the correlation between the dropping rate and EE% is also critical. At a dropping rate of 0.6 mL min^{-1}, the encapsulation efficiencies of ADE and COR were 75.3% and 70.7%, respectively. This indicates that the suitable dropping rate not only affects particle size but also enhances the loading bioactive compounds into the liposomes. Consequently, the injection rate of 0.6 mL min^{-1} was selected for following studies.

3.1.3. Effect of ultrasonic capacity. Ultrasonication plays a pivotal role in the preparation of nano-liposome systems and emulsions due to its ability to generate ultrasonic waves, which reduce particle size and enhance dispersion.[33] The phenomenon of cavitation occurs when ultrasonic waves create pressure variations, leading to the formation and collapse of small gas bubbles.[34,35] This generates strong shear forces and localized high temperatures, which not only improve dispersion efficiency but also promote the formation of uniform particles.[36] Optimizing the ultrasonic power is crucial to maximize these effects while maintaining the stability of the final product.

In this study, the ultrasonic power was investigated at 30%, 40%, 50%, 60%, 70%, and 80% of the device's maximum capacity. Fig. 1B and Table S2† illustrate the influence of ultrasonic power on both EE% and Z-average. The experimental data revealed that within the 50–60% power range, the EE% of both ADE and COR reached optimal levels. Specifically, the encapsulation efficiency of ADE increased from 63.7% (at 30%) to 75.7% (at 60%), while that of COR increased from 62.7% (at 30%) to 73.7% (at 60%). Concurrently, the Z-average decreased from 178.3 nm (at 30%) to a minimum of 108.3 nm (at 60%), indicating a high degree of uniformity.

However, when the ultrasonic power exceeded 60%, the encapsulation efficiency began to decline. At 80% power, the encapsulation efficiency of ADE dropped to approximately 66.7%, and that of COR decreased to 62.7%. This reduction can be attributed to the excessive ultrasonic power causing some LCMs particles to fragment into smaller phospholipid pieces, leading to the leakage of active compounds and a subsequent decrease in encapsulation efficiency. Statistical analysis of the data, as shown in the graph, confirmed that the differences between the power groups were statistically significant at $p < 0.05$. Therefore, an ultrasonic power of 60% was selected to best balance both EE% and particle size for next studies.

3.1.4. Effect of sonication time. In this section, the influence of sonication time at 60% power on the EE% and Z-average of the LCMs system was investigated in detail. Fig. 1C and Table S3† show that the particle size decreased significantly from 165.7 ± 5.1 nm (at 30 seconds) to 84.7 ± 6.1 nm (at 120 seconds), with statistically significant differences indicated by the letters on the graph ($p < 0.05$). This demonstrates that ultrasonication effectively breaks down larger aggregates into smaller particles. These observations align with the findings of Asadi et al.[37] and Amrollahi et al.[38] who similarly reported that extended sonication promotes the formation of individual nanoparticles by disrupting larger aggregates. Specifically,

sonication reduces the size of nanoparticle clusters, potentially separating them into individual particles. However, the reduction in particle size does not necessarily correlate with optimal encapsulation efficiency. The EE% reached its maximum at 60 seconds, with values of 72.7 ± 3.2% for ADE and 75.7 ± 3.8% for COR. When the sonication time was increased to 75 seconds and 90 seconds, the encapsulation efficiency began to decline, and this reduction became more pronounced at 120 seconds, with values of 54.3 ± 5.1% for ADE and 51.0 ± 1.0% for COR. Statistical analysis confirmed that this decrease was significant ($p < 0.05$). This phenomenon can be attributed to the excessive disruption of the liposome structure, leading to uncontrolled release of the active compounds from the liposomes.

Notably, at 120 seconds, both the encapsulation efficiency and particle size decreased significantly. The reduction in encapsulation efficiency at this time point suggests that prolonged sonication not only reduces particle size but also destabilizes and disrupts the liposome structure, ultimately compromising the delivery system's efficiency. These results confirm that a sonication time of 60 seconds is appropriate for subsequent experiments.

3.2. Characterization of the LCMs

Table 1 provides a comprehensive description of the properties of the LCMs suspension. The encapsulation efficiencies for ADE and COR under selected conditions were 72.7 ± 3.2% and 75.7 ± 3.8%, respectively. These results are comparable to those reported by Shashidhar Gkhi et al. who achieved EE% of 75.48 ± 2.5% for ADE, 74.9 ± 2.1% for COR, and 70.23 ± 2.9% for polysaccharides using a supercritical gas anti-solvent (SC-GAS) method to encapsulate Cordyceps extract within liposomes.[18] Our efficiencies are notably higher than those obtained by Annesha Roy et al. who used a bovine serum albumin and chitosan system to encapsulate free COR and *Cordyceps militaris* extract, reporting COR encapsulation efficiencies of 52.56% and 62.07%, respectively.[39] However, Khuntawee et al. demonstrated superior encapsulation, reaching 99% efficiency using microfluidic hydrodynamic focusing (MHF) with liposomes composed of a 10 : 1 molar ratio of egg yolk phosphatidylcholine to cholesterol.[19] These results highlight the dependence of encapsulation efficiency on the specific method employed, the composition of the liposomes, and the purity of the target compounds.

Table 1 Key parameters of the nano-LCMs suspension per 100 mL

Property	Parameter
Color, clarity	Yellowish-brown, transparent
EE of ADE (%)	72.7 ± 3.2
EE of COR (%)	75.7 ± 3.8
Z-Average (nm)	100.3 ± 1.5
PDI (a.u.)	1.346 0.014
ZP (mV)	−43.6 ± 0.3
Total ADE content (mg)	7.7 ± 0.8
Total COR content (mg)	12.8 ± 0.7
LC content (g)	0.4

After synthesis under optimized conditions, the nano-LCMs exhibited a homogeneous state with no phase separation or aggregation, displaying an excellent Tyndall effect (Fig. 2A). The morphology of the system, as observed by TEM image (Fig. 2B), revealed that the liposome nanoparticles were spherical in shape. The particle size distribution, measured by DLS method, ranged from 80 to 150 nm, with an average size of 100.3 nm (Fig. 2C). This size distribution was consistent with the TEM data, confirming the accuracy of the measurements. The PDI of the system was determined to be 0.346 a.u., indicating a uniform dispersion of particles.

In the FT-IR spectrum, the extract showed characteristic vibrations of –OH and –NH$_2$ groups in the 3200–3600 cm^{-1} region. Lecithin exhibited a characteristic phosphate group vibration at 1740 cm^{-1}, while the LCMs system displayed functional groups characteristic of both the *Cordyceps militaris* extract and lecithin. Specifically, the stretching vibration band at 3445 cm^{-1} was attributed to the –OH group.[40] Additionally, the keto (C=O) stretching vibration of the nano-system (1645 cm^{-1}) was narrower compared to that of the extract (1650 cm^{-1}) and lecithin (1740 cm^{-1}). In the LCMs system, the key functional groups were preserved, and changes in intensity suggested physical interactions between the core and shell.

In summary, when comparing the characteristic peaks in the FTIR spectra of the LCMs system with those of its individual components, the results indicated similarities in peak position, shape, and intensity. This confirms that the key functional groups of the organic compounds were retained during nano-system formation, allowing them to maintain their bioactivity when encapsulated in the LCMs system.

Another critical parameter for evaluating the properties of the nano-system is the ZP. The ZP reflects the electrical charge balance of charged particles in a solution and serves as an indicator of dispersion stability. It specifically represents the surface charge properties of nanoparticles. If the surface charge is sufficiently high, the particles repel each other, reducing the likelihood of aggregation and enhancing stability. A higher absolute value of the zeta potential predicts greater stability due to increased electrostatic repulsion between similarly charged particles, while a lower value suggests reduced stability. In practice, a nano-dispersion with a ZP absolute value between 30 and 60 mV achieves electrostatic stability due to repulsive forces between similarly charged nanoparticles. If the value ranges from 5 to 15 mV, the stability of the dispersion is limited, and a ZP between 3 and 5 mV often indicates instability.[41]

The ZP of the LCMs was measured at −43.6 mV, as shown in Fig. 2C, indicating high stability of the system. According to several studies, a negative zeta potential enhances the stability of nano-liposome systems.[41–43] Lipid-based nanoparticles, such as liposomes, typically exhibit a negative zeta potential due to the presence of phospholipids like phosphatidylcholine.[44] Other studies have shown that lipid-based nano-systems, such
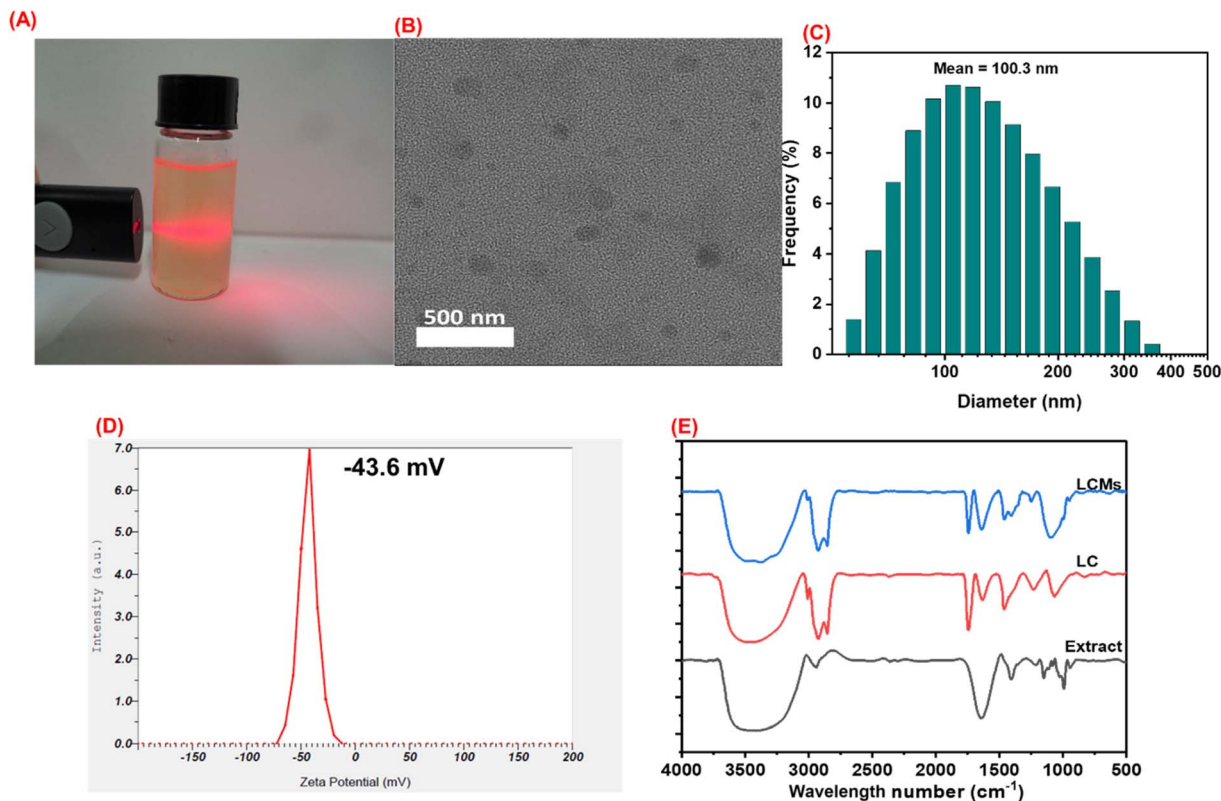

Fig. 2 Characteristics of the LCMs, (A): Photograph of the LCMs sample demonstrating the Tyndall effect (diluted with water at a 1 : 10 ratio), (B): morphology of LCMs particles observed using Transmission Electron Microscopy (TEM), (C): particle size distribution by DLS, (D): zeta potential, (E): FTIR spectra of the individual components and the LCMs system.

as solid lipid nanoparticles (SLNs) and nanostructured lipid carriers (NLCs), can form a negative ZP to improve absorption and stability.[42,45] Additionally, the interaction between ions and the lipid–water interface can lead to changes in the ZP of phospholipid vesicles, resulting in the formation of a negative surface charge under certain conditions.[46]

3.3. Stability

The stability of liposomes plays a crucial role in maintaining their structural integrity. Instability in liposomes can lead to uncontrolled fusion, unintended payload leakage, reduced shelf life, and unwanted mixing.[47] Furthermore, liposomes are susceptible to both physical and chemical degradation, which can diminish the efficiency and quality of the formulation, potentially resulting in product degradation and adverse side effects. Factors such as temperature, pH, surface charge, and lipid composition significantly influence the stability of liposomes.[48] To address these challenges, various strategies have been developed to enhance liposome stability, including drying techniques such as freeze drying, spray drying, spray-freeze drying, electrohydrodynamic methods, and supercritical

approaches, which are considered effective solutions for liposome preservation.[49] In this section, we focus on to investigate the effects of temperature, salt concentration, and storage duration on the stability of LCMs systems.

3.3.1. Effect of temperature. For the application of the LCMs system in food products, it is essential that the system exhibits thermal stability during heat processing. Temperature can influence the phase state of the lipid bilayer in liposomes, thereby affecting their permeability and drug release properties. In this study, the system was tested at temperatures of 50 °C and 90 °C. The results, as shown in Fig. 3A, indicate that the particle size distribution of the LCMs increased correspondingly with temperature. This can be explained by the fact that as temperature rises, the lipid membrane transitions from a gel state to a liquid state, increasing permeability and altering the particle size of the liposomes.[50] However, the average particle size of the system remained below 150 nm after heat treatment, demonstrating its potential for real applications.

3.3.2. Effect of ionic strength. NaCl plays a significant role in the stability of nano-systems. Therefore, understanding the stability of biological systems like liposomes in salt solutions of varying concentrations is crucial. The interaction between
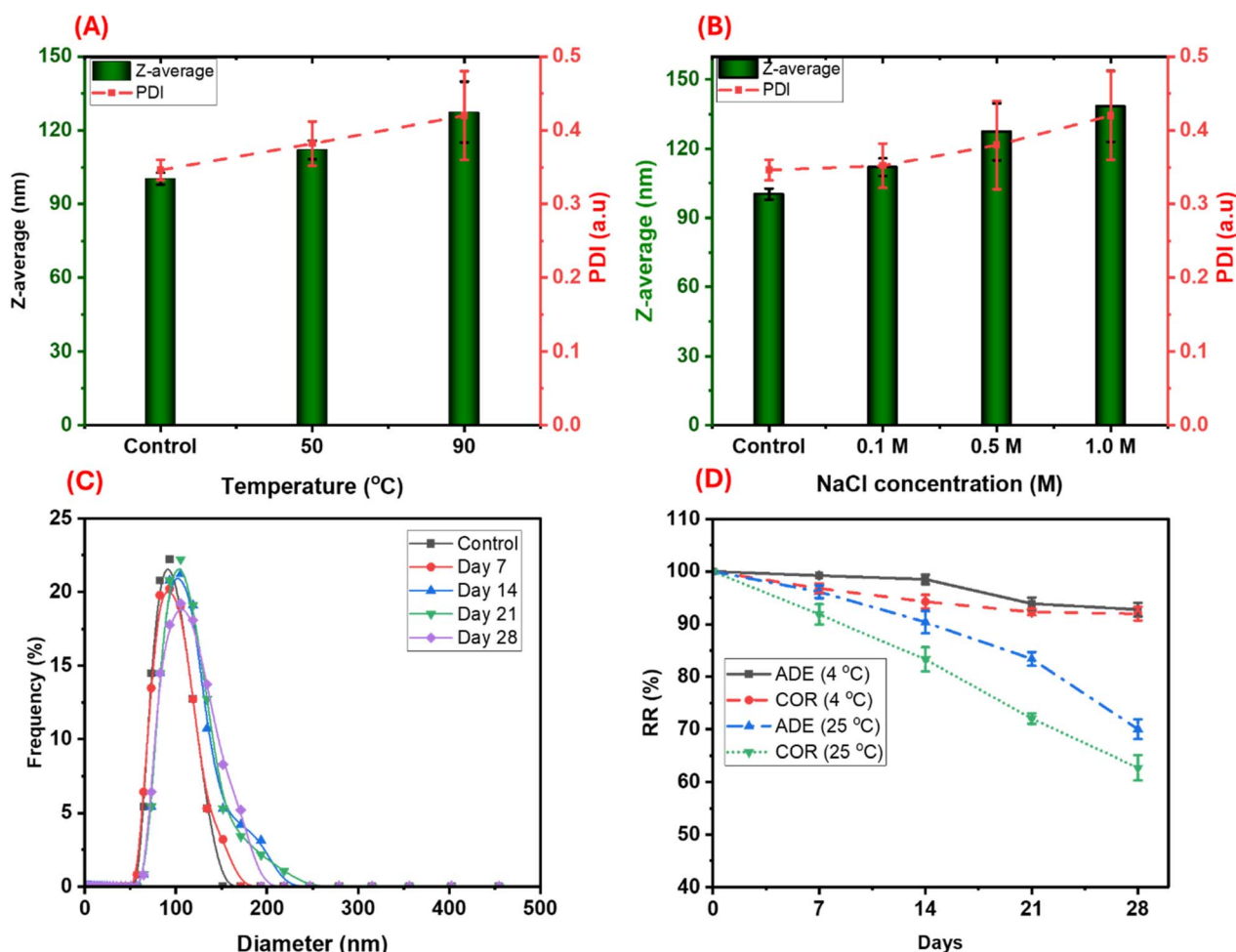

Fig. 3 (A) Mean diameter of the LCMs under heat treatment, (B) mean diameter of the LCMs in salt environments at different concentrations, (C): particle size distribution of the LCMs after storage at 4 °C, (D) retention of active compounds after storage at 4 °C and 25 °C.

         © 2025 The Author(s). Published by the Royal Society of Chemistry

liposomes and ions in a salt environment can affect their structure, properties, and encapsulation efficiency. The results, depicted in Fig. 3B, show that at all three salt concentrations, the particle size distribution of the LCMs changed, although the average particle size remained below 140 nm, and the polydispersity index (PDI) did not exceed 0.4.

Typically, liposomes lose water and shrink as ion concentration increases. According to Sabın et al. when the Na^+ concentration gradient increases, strong osmotic forces cause liposomes to shrink to balance osmotic pressure.[51] This mechanism may be due to changes in the charge of the lipid bilayer caused by ion adsorption on the membrane surface, altering the charge of the polar head groups and the membrane curvature. Additionally, the liposome membrane may be impermeable to certain ions, creating an osmotic pressure gradient across the membrane. As a result, water inside the liposome is expelled, leading to a reduction in size.[52] However, in this experiment, the particle size of the liposomes exhibited a slight increase in higher salt concentrations. This could be attributed to a reduction in surface tension, causing liposome particles to aggregate and leading to lipid clustering, which slightly increased the average size of the LCMs at higher salt concentrations.

3.3.3. Effect of storage time. Liposomes loaded with nutraceuticals offer slow release and high storage stability, enhancing their suitability for various applications.[53] To ensure these benefits are realized, it is crucial to conduct stability tests on produced liposomes to evaluate potential leakage and clustering during storage. As illustrated in Fig. 3C, after 4 weeks of storage, the shape of the size distribution graph remained almost unchanged, and the average particle size remained nearly constant (approximately 100 nm). Visual observations confirmed that the color of the liposome system showed no significant changes over the 28-day period. In contrast, when stored at room temperature (25 °C), the particle size exhibited a slight increase, reaching 139.5 ± 2.1 nm after 28 days of storage. However, the system remained stable without phase separation or sedimentation. These results demonstrate the long-term stability of the LCMs system under refrigerated conditions, highlighting its suitability for applications requiring extended storage.

Fig. 3D also demonstrates the EE% of ADE and COR within the LCMs system during refrigerated storage. After 30 days of storage at 4 °C, the retention rates of ADE and COR in the LCMs showed minimal changes (97.38% and 91.9%, respectively). However, at 25 °C, the retention rates of ADE and COR decreased significantly, reaching 75.44% and 62.38%, respectively. The decline in retention over time can be attributed to several factors. On one hand, liposomes are susceptible to oxidation during prolonged storage. After oxidation, liposomes tend to swell and form complex macromolecular structures, altering their surface properties.[54] This oxidation process can disrupt the ester bonds in phosphatidylcholine, leading to the release of encapsulated compounds. On the other hand, the observed increase in particle size is likely due to the thermal aggregation of the hydrophilic layer on the surface of the phospholipid bilayer, which can also deform the liposome structure and release the encapsulated active ingredients.[55,56]

Some authors have also reported that storage temperature affects the encapsulation efficiency of target compounds. For example, G. M. Shashidhar et al. indicated that the EE% of liposomes for adenosine, cordycepin, and polysaccharides decreased by less than 2.3% at 4 °C, 4.4% at 25 °C, and 9.8% at 37 °C after one month, and by less than 3.2% at 4 °C, 7.3% at 25 °C, and 20.3% at 37 °C after two months.[18] Similarly, Ji et al. used liposomes to co-encapsulate rutinoside and β-carotene modified by rhamnolipid. After 30 days, they observed that the retention of rhamnolipid-modified β-carotene (RL-βC) and rhamnolipid-modified β-carotene with rutinoside (RL-βC-Rts) decreased to 81.57 ± 1.48% and 85.2 ± 1.21% at 4 °C, and to 76.32 ± 1.33% and 79.21 ± 0.62% at 25 °C.[26] These collective findings suggest that liposome storage at 4 °C minimizes compound leakage, ensuring ADE and COR retention within the nano-liposomes.

3.4. Antioxidant activity

The antioxidant activity of a substance is evaluated based on its ability to scavenge DPPH free radicals, with antioxidants typically donating hydrogen atoms or electron pairs to neutralize these radicals. As illustrated in Fig. 4, the antioxidant activity of the LCMs system increased with concentration. At a concentration of 6.25 mg mL^{-1}, the LCMs system neutralized 84% of the free radicals, demonstrating its strong antioxidant potential, although it was still lower than that of the positive control, Trolox (IC50 143.21 µg mL^{-1}). These results indicate that the LCMs system exhibits excellent antioxidant properties, demonstrating higher antioxidant activity compared to the raw extract (IC50 2.89 vs. 7.23). This enhanced activity may be attributed, in part, to the intrinsic free radical scavenging properties of the liposome's lipid membrane.[57] Additionally, the antioxidant capacity of liposome systems is influenced by the encapsulated compounds, even those within the aqueous
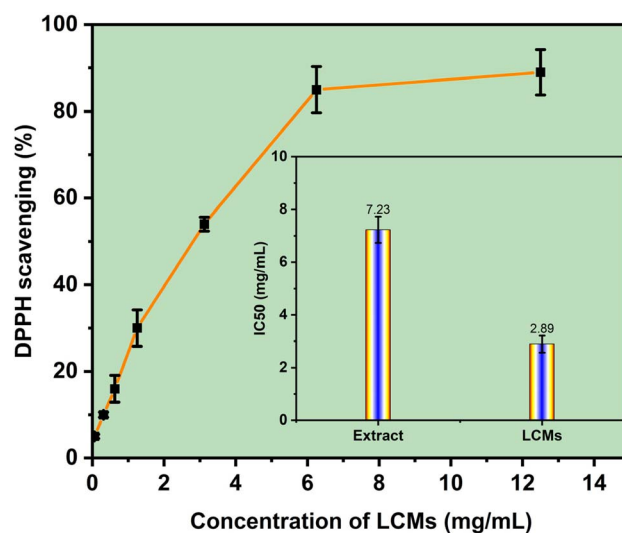

Fig. 4 DPPH free radical scavenging activity of the LCMs system at various concentrations, along with the IC50 values of the LCMs system compared to the extract.

phase. Luo *et al.* demonstrated that liposomes encapsulating procyanidins from lychee pericarp exhibit greater antioxidant capacity,[58] while Liu *et al.* showed a stronger antioxidant effect for vitamin C complex liposomes.[25] Ying Ji *et al.* also reported that rutinoside (Rts), a water-soluble compound located within the aqueous core of liposomes, exhibited higher DPPH scavenging activity than its free form.[26] Given that ADE and COR contain multiple –OH and –NH groups, known for their potent free radical scavenging capabilities. Upon exposure to free radicals, the lipid membrane of the LCMs system initially interacts with DPPH radicals. Subsequently, ADE and COR may migrate to interact with the lipid membrane, facilitating electron transfer across the membrane to neutralize the DPPH radicals. Finally, partial disruption of the lipid membrane may occur, allowing direct contact between ADE and COR molecules and the DPPH radicals for complete neutralization. Additionally, the nanoscale size of the system facilitates faster and more efficient antioxidant reactions due to the larger surface area available for interaction with free radicals, as previously reported in our studies.[22,33,59] Furthermore, liposome encapsulation protects ADE and COR from external factors such as light, heat, and oxygen, thereby maintaining their stability and antioxidant efficacy. Therefore, the results suggest that the *Cordyceps* extract was successfully encapsulated by the lipid material, retaining its biological activity and strong antioxidant capacity.

3.5. *In vitro* release performance in simulated digestion

To elucidate the potential applications of LMCs, the release behavior of ADE and COR was investigated using an *in vitro* simulated gastrointestinal digestion model. As presented in Fig. 5, in the absence of encapsulation, experimental results for the unencapsulated extract (control) demonstrated a rapid release of both ADE and COR. Over 80% of the active

compounds were released within the first 30 min of simulated gastric digestion, with near-complete release observed by the end of this phase.

In contrast, at the conclusion of simulated gastric digestion for the LMCs formulation, the cumulative release of ADE and COR remained below 20%. This notably limited release can be attributed to several factors. First, the simulated gastric fluid lacks the specific enzymes necessary to efficiently disrupt phospholipid bilayers, which form the structural basis of the LMCs. Furthermore, the sustained integrity of the LMCs structures throughout the simulated gastric digestion likely contributed to this phenomenon, as demonstrated in previous research with similar liposomal formulations.[25,60]

For the digestion process in the SIF model, the LMC formulations demonstrated a significant and desirable increase in the release of ADE and COR. The cumulative release rates of ADE and COR in the intestinal environment reached 87.11% and 85.14%, respectively, indicating efficient release under these conditions. This finding is consistent with previous studies. For instance, Ji *et al.* reported that after 4 hours of *in vitro* simulation intestinal fluids the cumulative release of β-carotene from liposomes reached 74.54%.[26] Similarly, Liu *et al.* reported that the cumulative release rate of β-carotene from liposome after 4 hours of gastrointestinal digestion was approximately 76.90%.[25] The significant increase in release in the intestinal environment may be attributed to two main factors: (1) the presence of lipolytic enzymes in pancreatin, which effectively hydrolyze the phospholipids constituting the LMC structure, and (2) the emulsifying action of bile salts on the liposome membranes.[61,62] Lipolytic enzymes facilitate chemical disruption of the phospholipid assemblies through hydrolysis, while bile salts promote the solubilization of intact LMCs into smaller vesicles and mixed micelles.[23]

These results indicate that the liposome shell effectively protects ADE and COR within the gastric environment *via* its lipid layer, while also regulating their release in the intestinal environment. This confirms the potential application of LCMs in the development of functional food products containing ADE and COR, especially in complex digestive environments. Overall, these findings highlight the capacity of LMCs to protect and deliver ADE and COR to the small intestine.

4. Conclusion

In conclusion, this study successfully developed a nanoliposome system encapsulating ADE and COR from *Cordyceps militaris* extract, demonstrating its potential to enhance the bioavailability and stability of these bioactive compounds. Using an optimized solvent injection method, liposomes with an average particle size of 100.3 nm and encapsulation efficiencies (72.7 ± 3.2% for ADE and 75.7 ± 3.8% for COR) were achieved. The system exhibited exceptional long-term stability under refrigerated conditions, with minimal changes in particle size and zeta potential over 28 days. Additionally, the nanoliposomes displayed superior antioxidant activity, outperforming the raw extract in DPPH radical scavenging assays. The liposome LCMs shell effectively protected ADE and COR in
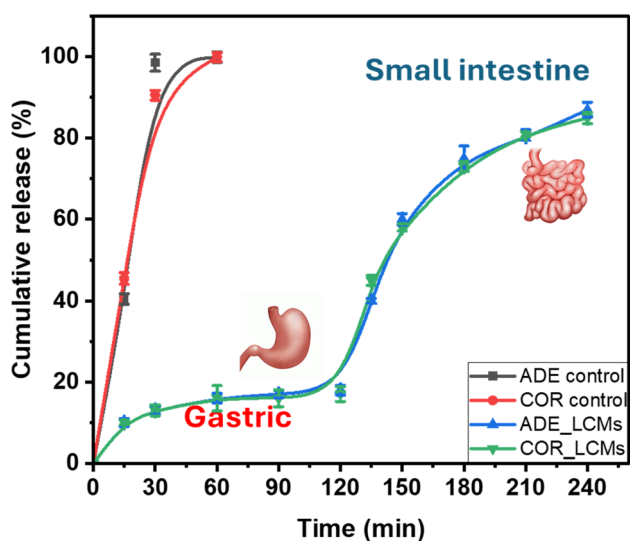

Fig. 5 Cumulative release curves of ADE and COR from extract and LMCs during *in vitro* gastrointestinal digestion simulated at 37 °C (where squares and circles represent the release of ADE and COR from the extract (control), and triangles represent the release from LMCs).

the gastric environment through its lipid layer while precisely controlling their release in the intestinal environment. These findings open new avenues for the application of nano-liposomes in functional foods and pharmaceutical products, providing a robust platform to maximize the health benefits of *Cordyceps militaris*. Future research will focus on developing powdered formulations of the nano-liposome system using freeze-drying and spray-drying techniques, as well as exploring its potential in supplement and funtional food applications.

Data availability

All data supporting the findings of this study are available within the article and its ESI.† Raw data, including experimental protocols, analytical results, and characterization data, are available from the corresponding author upon reasonable request.

Author contributions

Conflicts of interest

The authors declare that they have no known competing financial interests or personal relationships that could have appeared to influence the work reported in this paper.

Acknowledgements

References

1 S. Shweta, K. Abdullah and A. Kumar, *Pharmacol Res.–Modern Chinese Med.*, 2023, **7**, 100228.

2 H. S. Tuli, S. S. Sandhu and A. K. Sharma, *3 Biotech*, 2014, **4**, 1–12.

3 K. Yue, M. Ye, Z. Zhou, W. Sun and X. Lin, *J. Pharm. Pharmacol.*, 2013, **65**, 474–493.

4 G. Haskó, L. Antonioli and B. N. Cronstein, *Biochem. Pharmacol.*, 2018, **151**, 307–313.

5 G. Yu, J. Peng, L. Li, W. Yu, B. He and B. Xie, *Braz. J. Med. Biol. Res.*, 2024, **57**, e13889.

6 Q. Deng, X. Li, C. Fang, X. Li, J. Zhang, Q. Xi, Y. Li and R. Zhang, *Int. Immunopharmacol.*, 2022, **107**, 108695.

7 Z. Zhang, K. Li, Z. Zheng and Y. Liu, *BMC Pharmacol. Toxicol.*, 2022, **23**, 12.

8 H. Cai, J. Li, B. Gu, Y. Xiao, R. Chen, X. Liu, X. Xie and L. Cao, *J. Ethnopharmacol.*, 2018, **214**, 106–112.

9 H. Tang, C. Chen, Y. Zou, H. Lou, Q. Zheng, L. Guo, J. Lin, Z. Ye and F. Yun, *Appl. Microbiol. Biotechnol.*, 2019, **103**, 7943–7952.

10 Y. Xia, F. Luo, Y. Shang, P. Chen, Y. Lu and C. Wang, *Cell Chem. Biol.*, 2017, **24**, 1479–1489e4.

11 Y.-J. Tsai, L.-C. Lin and T.-H. Tsai, *J. Agric. Food Chem.*, 2010, **58**, 4638–4643.

12 E. Moreno, J. Canet, E. Gracia, C. Lluís, J. Mallol, E. I. Canela, A. Cortés and V. Casadó, *Front. Pharmacol.*, 2018, **9**, 106.

13 J. B. Lee, M. Radhi, E. Cipolla, R. D. Gandhi, S. Sarmad, A. Zgair, T. H. Kim, W. Feng, C. Qin, C. Adrower, C. A. Ortori, D. A. Barrett, L. Kagan, P. M. Fischer, C. H. de Moor and P. Gershkovich, *Sci. Rep.*, 2019, **9**, 15760.

14 C. Corciulo, C. M. Castro, T. Coughlin, S. Jacob, Z. Li, D. Fenyö, D. B. Rifkin, O. D. Kennedy and B. N. Cronstein, *Sci. Rep.*, 2020, **10**, 13477.

15 R. Eugster and P. Luciani, *Curr. Opin. Colloid Interface Sci.*, 2025, **75**, 101875.

16 H. He, Y. Lu, J. Qi, Q. Zhu, Z. Chen and W. Wu, *Acta Pharm. Sin. B*, 2019, **9**, 36–48.

17 E. J. Rupa, J. F. Li, M. H. Arif, H. Yaxi, A. M. Puja, A. J. Chan, V. A. Hoang, L. Kaliraj, D. C. Yang and S. C. Kang, *Molecules*, 2020, **25**(23), 5733.

18 G. M. Shashidhar and B. Manohar, *RSC Adv.*, 2018, **8**, 34634–34649.

19 W. Khuntawee, R. Amornloetwattana, W. Vongsangnak, K. Namdee, T. Yata, M. Karttunen and J. Wong-ekkabut, *RSC Adv.*, 2021, **11**, 8475–8484.

20 T. T. Nguyen, D. V. Nguyen, Q. H. Tran, M. D. Pham, V. M. Nguyen, T. T. Nguyen, C. D. Tran and T. D. Nguyen, *J. Mol. Liq.*, 2024, **397**, 124107.

21 C. P. Huynh, T. P. Pham, M. K. Nguyen and Q. H. Tran, *Acta Chem. Iasi*, 2024, **32**, 207–236.

22 Q. H. Tran, H. K. T. Chu, P. T. Nguyen, V. M. Nguyen, Q. T. Nguyen, C. D. Tran and T. D. Nguyen, *ACS Food Sci. Technol.*, 2023, **3**, 2229–2237.

23 K. Tai, M. Rappolt, L. Mao, Y. Gao and F. Yuan, *Food Chem.*, 2020, **326**, 126973.

24 L. Zhao, D. Wang, J. Yu, X. Wang, T. Wang, D. Yu and W. Elfalleh, *Food Biosci.*, 2024, **61**, 104899.

25 X. Liu, P. Wang, Y.-X. Zou, Z.-G. Luo and T. M. Tamer, *Food Res. Int.*, 2020, **136**, 109587.

26 Y. Ji, Z. Wang, X. Ju, F. Deng, F. Yang and R. He, *J. Food Sci.*, 2023, **88**, 2064–2077.

27 N. Q. Thang, V. T. K. Hoa, L. Van Tan, N. T. M. Tho, T. Q. Hieu and N. T. K. Phuong, *Vietnam J. Chem.*, 2022, **60**, 571–577.

28 Y. Wu, Y. Luo and Q. Wang, *LWT–Food Sci. Technol.*, 2012, **48**, 283–290.

29 L. Zhao, F. Temelli, J. M. Curtis and L. Chen, *Food Res. Int.*, 2015, **77**, 63–72.

30 E. Jaradat, E. Weaver, A. Meziane and D. A. Lamprou, *Nanomaterials*, 2021, **11**, 3440.

31 Z. T. Rushmi, N. Akter, R. J. Mow, M. Afroz, M. Kazi, M. de Matas, M. Rahman and M. H. Shariare, *Saudi Pharm. J.*, 2017, **25**, 404–412.

32 J. Song, F. Shi, Z. Zhang, F. Zhu, J. Xue, X. Tan, L. Zhang and X. Jia, *Molecules*, 2011, **16**, 7880–7892.

33 Q. H. Tran, T. T. H. Thuy and T. T. T. Nguyen, *New J. Chem.*, 2021, **45**, 9658–9667.

34 M. Ashokkumar, *Ultrason. Sonochem.*, 2011, **18**, 864–872.

35 H. T. T. Thuy, P. T. K. Ngoc, N. T. T. Tu, H. T. T. Truc, N. Van Hai and T. Q. Hieu, *J. Sci. Technol.*, 2019, **39A**(3), 57–65.

36 K. Sakthipandi, B. Sethuraman, K. Venkatesan, B. Alhashmi, G. Purushothaman and I. A. Ansari, in *Handbook of Vibroacoustics, Noise and Harshness*, Springer Nature Singapore, Singapore, 2025, pp. 1117–1162.

37 A. Asadi, F. Pourfattah, I. Miklós Szilágyi, M. Afrand, G. Żyła, H. Seon Ahn, S. Wongwises, H. Minh Nguyen, A. Arabkoohsar and O. Mahian, *Ultrason. Sonochem.*, 2019, **58**, 104701.

38 A. Amrollahi, A. A. Hamidi and A. M. Rashidi, *Nanotechnology*, 2008, **19**, 315701.

39 A. Roy, C. C. Mate, K. Kumari, D. Khatak, A. K. Patel, R. M. Jeza Almotairi, S. Muthupandian and R. Meena, *Microb. Pathog.*, 2025, **205**, 107662.

40 N. Baran, V. K. Singh, K. Pal, A. Anis, D. K. Pradhan and K. Pramanik, *Polym.-Plast. Technol. Eng.*, 2014, **53**, 865–879.

41 R. Shah, D. Eldridge, E. Palombo and I. Harding, *J. Phys. Sci.*, 2014, **25**(1), 59–75.

42 L. Li, H. Wang, J. Ye, Y. Chen, R. Wang, D. Jin and Y. Liu, *Molecules*, 2022, **27**, 4408.

43 T. M. Taylor, S. Gaysinsky, P. M. Davidson, B. D. Bruce and J. Weiss, *Food Biophys.*, 2007, **2**, 1–9.

44 M. Socaciu, Z. Diaconeasa and C. Socaciu, *Studia UBB Chemia*, 2019, **64**, 181–192.

45 L. Benedini, S. Antollini, M. L. Fanani, S. Palma, P. Messina and P. Schulz, *Mol. Membr. Biol.*, 2014, **31**, 85–94.

46 A. Wolde-Kidan and R. R. Netz, *Langmuir*, 2021, **37**, 8463–8473.

47 P. Chowdhary, L. Mahalakshmi, S. Dutta, J. A. Moses and C. Anandharamakrishnan, in *Liposomal Encapsulation in Food Science and Technology*, Elsevier, 2023, pp. 223–237.

48 B. Roy, P. Guha, R. Bhattarai, P. Nahak, G. Karmakar, P. Chettri and A. K. Panda, *J. Jpn. Oil Chem. Soc.*, 2016, **65**, 399–411.

49 I. Andreana, V. Bincoletto, M. Manzoli, F. Rodà, V. Giarraputo, P. Milla, S. Arpicco and B. Stella, *Materials*, 2023, **16**, 1212.

50 W. Chen, F. Duša, J. Witos, S.-K. Ruokonen and S. K. Wiedmer, *Sci. Rep.*, 2018, **8**, 14815.

51 J. Sabın, G. Prieto, J. M. Ruso, R. Hidalgo-Álvarez and F. Sarmiento, *Eur. Phys. J. E:Soft Matter Biol. Phys.*, 2006, **20**, 401–408.

52 Q. Wang, W. Li, N. Hu, X. Chen, T. Fan, Z. Wang, Z. Yang, M. A. Cheney and J. Yang, *Colloids Surf., B*, 2017, **155**, 287–293.

53 T. Liang, R. Guan, H. Shen, Q. Xia and M. Liu, *Molecules*, 2017, **22**, 457.

54 M. A. Chaves, P. L. Oseliero Filho, C. G. Jange, R. Sinigaglia-Coimbra, C. L. P. Oliveira and S. C. Pinho, *Colloids Surf., A*, 2018, **549**, 112–121.

55 B. Budavári, Á. Karancsi, B. G. Pinke, É. Pállinger, K. Juriga-Tóth, M. Király, Z. Szász, I. Voszka, K. Molnár, L. Kőhidai, A. Jedlovszky-Hajdu and K. S. Nagy, *J. Mol. Liq.*, 2024, **394**, 123756.

56 R. Nemoto, K. Fujieda, Y. Hiruta, M. Hishida, E. Ayano, Y. Maitani, K. Nagase and H. Kanazawa, *Colloids Surf., B*, 2019, **176**, 309–316.

57 M. E. Nasab, N. Takzaree, P. M. Saffari and A. Partoazar, *J. Comp. Eff. Res.*, 2019, **8**, 633–643.

58 M. Luo, R. Zhang, L. Liu, J. Chi, F. Huang, L. Dong, Q. Ma, X. Jia and M. Zhang, *J. Food Eng.*, 2020, **284**, 110065.

59 Q. H. Tran, T. T. Le Thi, T. C. Nguyen, T. V. Tran, Q. T. Le, T. T. Luu and V. P. Dinh, *J. Food Process. Preserv.*, 2021, e15402.

60 K. Tai, X. He, X. Yuan, K. Meng, Y. Gao and F. Yuan, *Colloids Surf., A*, 2017, **518**, 218–231.

61 W. Liu, A. Ye, C. Liu, W. Liu and H. Singh, *Food Res. Int.*, 2012, **48**, 499–506.

62 A. Sadeghpour, M. Rappolt, S. Misra and C. V. Kulkarni, *Langmuir*, 2018, **34**, 13626–13637.